2009 American Control Conference
Hyatt Regency Riverfront, St. Louis, MO, USA
June 10-12, 2009

Vision-based Reactive Multiple Obstacle Avoidance for Micro Air Vehicles

Jeffery Saunders and Randal Beard
Brigham Young University, Provo, Utah, 84602
Jeffrey Byrne
500 West Cummings Park, Suite 3000, Woburn, MA 01801

***Abstract*— Traditional sensors for obstacle detection on aircraft, such as radar, are too heavy for fixed wing micro air vehicles and make obstacle detection and avoidance a difficult problem. EO/IR cameras are small and lightweight enough to offer an alternative to heavy sensors. Vision processing available on a ground station provides range and bearing to nearby obstacles. We propose a nonlinear guidance law based on movement of obstacles in the camera field-of-view to "push" the obstacles to the edge of the camera field-of-view and thus avoid collision. As the MAV passes obstacles, the original course is resumed. The guidance strategy is demonstrated in simulation and flight test. This reactive method intended for use in conjunction with high level path planners.**

I. Introduction

Automated obstacle detection and avoidance in micro air vehicles (MAV) is a difficult problem because of the need to reliably detect obstacles, compute trajectories quickly, and arrive at a goal in a timely manner while remaining within the flight constraints of the MAV. Undetected obstacles make flying in unknown environments dangerous. Reliable obstacle avoidance requires sensors that guarantee obstacle detection in the trajectory of the MAV to prevent collision and requires trajectory generators that create new paths around the obstacles. The new paths must arrive at the goal while satisfying nonholonomic constraints. While these objectives are difficult to achieve, the applications of obstacles avoidance are valuable as MAVs become commonplace in many different fields such as mapping terrains, surveillance, and search and rescue in all types of environments.

A common approach to obstacle avoidance is potential fields [2], [6], [25] which create artificial "forces" in response to nearby obstacles and goals. Obstacles generate a repulsive force, and goals generate an attractive force, which are a function of the current state and easily calculated in real time. Potential fields often create local minima and cannot guarantee obstacle avoidance. Another class of potential fields that remove local minima are called navigation functions, but are often difficult to compute [24]. A hybrid approach combining potential fields with other methods can remove the problem of local minima [18].

J. Saunders is a graduate research assistant, Electrical and Computer Engineering, Brigham Young University
R. Beard is a professor, Electrical and Computer Engineering, Brigham Young University
J. Byrne is a research engineer at Scientific Systems Company, Inc.

Probability Road Map (PRM) techniques can produce fast paths to goal with computation measured in seconds [1], [8], [9]. PRM methods randomly generate waypoints to span a configuration space. A sequence of waypoints are connected to the goal to avoid obstacles. The general PRM technique is designed for holonomic vehicles. A probabilistic planner with extensions to nonholonomic vehicles was developed in [4] called Rapidly-Expanding Random Trees (RRT). The RRT method is well suited to most nonholonomic constraints including a fixed-wing aircraft. The RRT generates random points in the configurations space and connects each configuration to a tree if the kinematic constraints of the vehicle and obstacle constraints do not prevent the movement from the first configuration to the second. As the tree grows through the configurations space, it eventually extends to the goal, connecting the initial configuration to the final configuration. The RRT has had many successful variants including narrow passageways, and smoothing techniques, and growing the tree from the initial condition and final configuration simultaneously [11]–[15], [22], [23]. The computation time in complex environments is usually in seconds, making randomized path planners excellent for replanning paths, but insufficient for reactive obstacle avoidance.

Cell decomposition is another popular path planning method in which a configuration space is decomposed into cells. A path is easily found in each cell. A sequence of cells is found to connect the initial conditions to the goal [16], [26]. Additional methods include visibility graphs [17], Voronoi diagrams [19], and Mixed integer linear programming (MILP) [21]. Each have varying success, though all have computation times too high for reactive obstacle avoidance.

Regardless of the method, there are four objectives to trajectory generation: 1) guarantee obstacle avoidance, 2) stay within the complex constraints of flight dynamics, 3) compute a new trajectory immediately upon detection of an obstacle in the current trajectory, an increase in computation time adds constraints to an already complex problem, and 4) arrive at the goal in close to minimal time or distance. In previous work, these objectives have been summarized as computation requirements and completeness [5].

Our contribution is a reactive guidance strategy within a tiered system of path planning to achieve the objectives of trajectory generation. Obstacles avoidance is best approached

978-1-4244-4524-0/09/$25.00 ©2009 AACC

in a multi-tiered system to better address each of the objectives. The trajectory generation system used in this paper will have three tiers. The first tier reacts instantaneously to detected obstacles using a reactive guidance strategy based on a feedback control law. The control law maneuvers the MAV to "push" the obstacles to the edges of the camera field-of-view essentially avoiding immediate collision with obstacles. The reactive method is the focus of this paper. The second tier plans a waypoint path around obstacles locally in the body frame of the MAV. The third tier creates a global path from the current configuration to the goal. Each tier acts at a different time scale and has increasing computation time. The reactive guidance responds to obstacles where the predicted time-to-collision is 0-5 seconds and requires very little computation. The tier two planner reacts to obstacles where the predicted time-to-collision is 5-30 seconds and plans a local path, it overrides the reactive planner. The tier three reacts to obstacles where the predicted time-to-collision is greater than 30 seconds and plans a global path to the goal. The global planner overrides the local planner. The tiered system achieves objectives 1 with constraints on the obstacles. Objectives 2 is met by each layer separately. Reactive avoidance satisfies objective 3 by reacting to obstacles by "pushing" them to the edge of the camera- field-of-view and objective 4 is achieved by path smoothing in the global path planner.

We use a camera to detect obstacles. Cameras are small and light-weight enough to mount on small MAVs. Airframe mounted cameras have the potential to provide range estimation, object segmentation, and object identification. Vision based obstacle detection is a topic of research and while it has not reached reliability for commercial aircraft systems, it continues to show potential [3], [10], [20]. In this paper, we assume a range map is available from vision processing on the ground station. A range and bearing estimation scheme will be presented in section IV.

The organization of this paper is as follows. Section II provides a description of the system and the obstacle avoidance problem. Section III introduces the guidance strategy followed by state estimation techniques in section IV. Simulation results are presented in V and flight results in VI with a conclusion in VII.

II. Problem Overview

The target airframe is a fixed wing MAV with wingspan less than 48 inches. The MAV is equipped with an onboard autopilot with inner loops on roll, pitch, and yaw angles. The autopilot maintains a constant airspeed and a constant altitude. Assuming zero wind, the kinematic model is given by

$$\dot{z}_n = V\cos\psi, \tag{1}$$
$$\dot{z}_e = V\sin\psi, \tag{2}$$
$$\dot{\psi} = \frac{g}{V}\tan\phi, \tag{3}$$

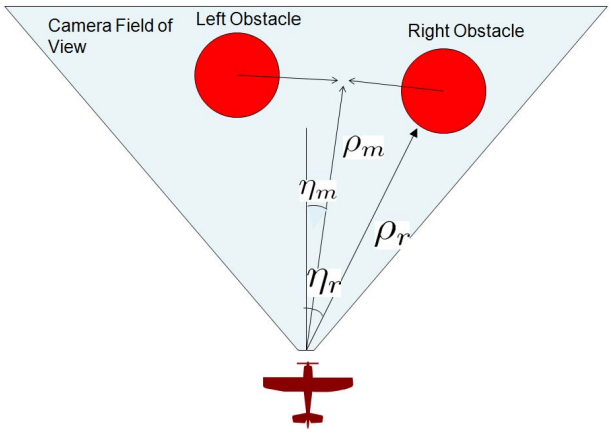

Fig. 1. A conceptual view of the MAV approaching 2 obstacles is shown. The objective of the control is to fly between the obstacles to avoid collision.

where $(z_n, z_e)^T$ is the North-East position of the MAV. The airspeed, yaw, and roll angles are defined as V, ψ, and ϕ respectively. The gravitational acceleration is represented by g. The camera is mounted parallel to the longitudinal axis of the body frame to allow it to capture obstacle data in the reachable region of the MAV in the $0-5$ second time frame.

Maps of terrain and potential obstacles within the terrains are often available before launch and are used to plan a trajectory to avoid collision. However, those maps may not be accurate, requiring a sensor to detect pop-up obstacles. We assume a range map is available by vision processing. A range estimation scheme is given in section IV.

III. Dynamics and Guidance Strategy

We will simplify multiple obstacle avoidance into the case of avoiding two obstacles at a time, a left obstacle and a right obstacle. Any set of obstacles with number greater than two can be subdivided into groups of two. Obstacles within a threshold distance τ of each other are too dangerous to fly between and are considered a single obstacle. In the case of a single obstacle, the method described in reference [7] can be used.

Let ρ_r and ρ_l denote the range to the right and left obstacles in the camera field-of-view. Let η_r and η_l be the bearing to the right and left obstacles. An illustration of the obstacles in relation to the MAV body frame and camera field-of-view is shown in Figure 1.

Let ρ_m and η_m be the range and bearing to the midpoint between the two obstacles where

$$\rho_m = \frac{\rho_r + \rho_l}{2},$$
$$\eta_m = \frac{\eta_r + \eta_l}{2}.$$

The midpoint is a static point and therefore moves as a static obstacles in the body frame. The dynamics of the obstacle in the MAV body frame are derived from equations (1)-(3) as

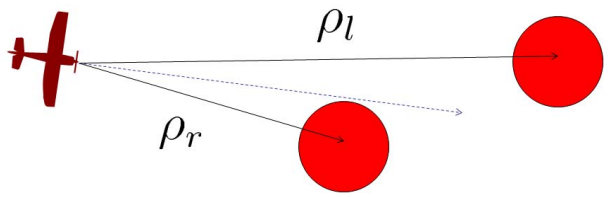

Fig. 2. If the MAV avoids the obstacles by only moving the obstacles to the edges of the image plane, the MAV may come in close proximity to the obstacle. To avoid this problem, force $\rho_r - \rho_l$ to zero as well.

$$\dot{\rho}_* = - V_a \cos \eta_*, \tag{4}$$
$$\dot{\eta}_* = \frac{V}{\rho_*} \sin \eta_* - \dot{\psi}. \tag{5}$$

where $*$ may denote right obstacle r, left obstacle l, or midpoint m.

Equation (3) relates the yaw rate $\dot{\psi}$ to the roll angle ϕ. Substituting (3) into (5) yields

$$\dot{\eta}_* = \frac{V_a}{\rho_*} \sin \eta_* - \frac{g}{V_a} \tan \phi. \tag{6}$$

The objective is to avoid both obstacles simultaneously. We will do this by balancing the obstacles on the sides of the image plane. In the absence of wind, the course angle of the MAV is the angle of the optical axis. Moving the obstacles to the edges of the camera field-of-view effectively moves the MAV off of a collision with an obstacle. Since the case is limited to two obstacles, the guidance strategy can "push" the obstacles to either side of the image plane.

Moving the obstacles to the edges of the image plane will not balance distance between them. If the MAV approaches the obstacles at a steep angle, as shown in Figure 2, it will come in close proximity to one of them, and possibly collide. To avoid this problem, we also need to drive the difference in range-to-obstacles $\rho_d = \rho_r - \rho_l$ to zero. If the control algorithm maintains $\rho_r = \rho_l$, then in the scenario in Figure 2 the MAV will roll away from the obstacles to force the ρ_d to zero while simultaneously driving η_m to zero.

The control needs to push the obstacles to opposite sides of the image plane. This can be done by driving η_m and ρ_d to zero simultaneously. We use backstepping to derive the guidance strategy. Consider the Lyapunov function candidate

$$W_1 = \frac{k_1}{2} \rho_d^2,$$

and differentiate it to obtain

$$\begin{aligned} \dot{W}_1 &= k_1 \rho_d \left(-V \cos \eta_r + V \cos \eta_l \right) \\ \dot{W}_1 &= k_1 \rho_d \left(-V \cos \left(2\eta_m - \eta_l \right) + V \cos \eta_l \right). \end{aligned} \tag{7}$$

Assume for the moment that η_m is a controllable input and let $\beta = \eta_m$ be the input, then

$$\dot{W}_1 = k_1 \rho_d \left(-V \cos \left(2\beta - \eta_l \right) + V \cos \eta_l \right).$$

Letting

$$\beta = \frac{1}{2} \left(\eta_l + \cos^{-1} \left(\cos \eta_l + \frac{k_1}{V} \rho_d \right) \right), \tag{8}$$

the Lyapunov function candidate simplifies to

$$\dot{W}_1 = - k_1^2 \rho_d^2.$$

Let $\zeta = \eta_m - \beta$ and introduce ζ as a change of variable. Differentiating ζ we obtain

$$\begin{aligned} \dot{\zeta} &= \dot{\eta_m} - \dot{\beta}, \\ &= \frac{V}{\rho_m} \sin \eta_m - \frac{g}{V} \tan \phi - \dot{\beta}, \end{aligned} \tag{9}$$

where

$$\begin{aligned} \dot{\beta} = \frac{1}{2} \Bigg[& \frac{V}{\rho_l} \sin \eta_l - \dot{\psi} - \frac{1}{\sqrt{1 - cos\eta_l - \frac{k_1}{V} \rho_d}} \\ & \left(- \sin \eta_l \left(\frac{V}{\rho_l} \sin \eta_l - \dot{\psi} \right) + k_1 \left(-cos\eta_r + cos\eta_l \right) \right) \Bigg] \end{aligned}$$

Let W_2 be the new Lyapunov candidate

$$W_2 = \frac{k_1}{2} \rho_d^2 + \frac{1}{2} \zeta^2.$$

Differentiating W_2 yields

$$\begin{aligned} \dot{W}_2 &= k_1 \rho_d \dot{\rho_d} + \zeta \dot{\zeta}, \\ &= k_1 \rho_d \left[-V \cos \left(2\eta_m - 2\beta - \eta_l + 2\beta \right) + V \cos \eta_l \right] + \zeta \dot{\zeta}, \\ &= k_1 \rho_d \left[-V \cos \left(2\zeta \right) \cos \left(2\beta - \eta_l \right) \right. \\ &\quad \left. + V \sin \left(2\zeta \right) \sin \left(2\beta - \eta_l \right) + V \cos \eta_l \right] + \zeta \dot{\zeta}, \\ &= k_1 \rho_d \Bigg[-V \cos \left(2\zeta \right) \left(\cos \eta_l + \frac{k_1}{V} \rho_d \right) \\ &\quad + V \sin \left(2\zeta \right) \sqrt{1 - \left(\cos \eta_l + \frac{k_1}{V} \rho_d \right)^2} \\ &\quad + V \cos \eta_l \Bigg] + \zeta \dot{\zeta}. \end{aligned}$$

Substitute infinite series for $\cos(2\zeta)$ and $\sin(2\zeta)$

$$\begin{aligned} \dot{W}_2 = k_1 \rho_d \Bigg[& -V \left(1 - \frac{(2\zeta)^2}{2!} + ... \right) \left(\cos \eta_l + \frac{k_1}{V} \rho_d \right) \\ & + V \left(2\zeta - \frac{(2\zeta)^3}{3!} + ... \right) \sqrt{1 - \left(\cos \eta_l + \frac{k_1}{V} \rho_d \right)^2} \\ & + V \cos \eta_l \Bigg] + \zeta \dot{\zeta}. \end{aligned}$$

By factoring out ζ and simplifying, the Lyapunov function becomes

$$\dot{W}_2 = k_1\rho_d\left[-V\left(\cos\eta_l + \frac{k_1}{V}\rho_d\right) + V\cos\eta_l\right] + \zeta\left[k_1\rho_d\left(-V\left(-\frac{2(2\zeta)}{2!} + \frac{2(2\zeta)^3}{4!} + ...\right)\left(\cos\eta_l + \frac{k_1}{V}\rho_d\right) + V\left(2 - \frac{2(2\zeta)^2}{3!} + ...\right)\sqrt{1-\left(\cos\eta_l + \frac{k_1}{V}\rho_d\right)^2}\right) + \dot{\zeta}\right],$$

$$\dot{W}_2 = -k_1^2\rho_d^2 + \zeta\left[2k_1\rho_d V\left(\sum_{i=0}^{\infty}\frac{(2\zeta)^{2i+1}(-1)^i}{(2i+2)!}\left(\cos\eta_l + \frac{k_1}{V}\rho_d\right) + \sum_{i=0}^{\infty}\frac{(2\zeta)^{2i}(-1)^i}{(2i+1)!}\sqrt{1-\left(\cos\eta_l + \frac{k_1}{V}\rho_d\right)^2}\right) + \dot{\zeta}\right]. \quad (10)$$

Substituteing (9) for $\dot{\zeta}$ into (10) gives

$$\dot{W}_2 = -k_1^2\rho_d^2 + \zeta\left[2k_1\rho_d V\left(\sum_{i=0}^{\infty}\frac{(2\zeta)^{2i+1}(-1)^i}{(2i+2)!}\left(\cos\eta_l + \frac{k_1}{V}\rho_d\right) + \sum_{i=0}^{\infty}\frac{(2\zeta)^{2i}(-1)^i}{(2i+1)!}\sqrt{1-\left(\cos\eta_l + \frac{k_1}{V}\rho_d\right)^2}\right) + \frac{V}{\rho_m}\sin\eta_m - \frac{g}{V}\tan\phi - \dot{\beta}\right]. \quad (11)$$

The control input in equation (11) is the roll angle ϕ. To stabilize the system, let

$$\phi = \tan^{-1}\left[\frac{V}{g}\left(\frac{V}{\rho_m}\sin\eta_m - \dot{\beta} + k_2\zeta + 2k_1\rho_d V\left(\sum_{i=0}^{\infty}\frac{(2\zeta)^{2i+1}(-1)^i}{(2i+2)!}\left(\cos\eta_l + \frac{k_1}{V}\rho_d\right) + \sum_{i=0}^{\infty}\frac{(2\zeta)^{2i}(-1)^i}{(2i+1)!}\sqrt{1-\left(\cos\eta_l + \frac{k_1}{V}\rho_d\right)^2}\right)\right)\right], \quad (12)$$

which results in the negative definite Lyapunov function

$$\dot{W}_2 = -k_1^2\rho_d^2 - k_2\zeta^2. \quad (13)$$

Notice that $\cos^{-1}$ limits the range of the system to $-1 < \cos\eta_r + \frac{k_1}{V}\rho_d < 1$.

The guidance strategy must guide the MAV to a path that avoids obstacles. The following theorem proves that the control law in equation (12) guides the MAV to the perpendicular bisector of the two obstacles.

Theorem 3.1: If two obstacles are avoided using the guidance strategy in equation (12), then the MAV approaches the perpendicular bisector of the two obstacles described by the line $\rho_r = \rho_l$.

Proof: The Lyapunov function (13) proves that $\rho_d \to 0$ and $\eta_m \to 0$ simultaneously. If $\rho_d = 0$, then $\rho_r = \rho_l$ implying the MAV is on the perpendicular bisector. If $\eta_m = 0$ as well, then $\phi = 0$. The kinematic equations show that $\dot{\eta}_m = 0$ and $\dot{\rho}_d = \dot{\rho}_r - \dot{\rho}_l = 0$ implying that the perpendicular bisector is an invariant set. Equation (13) is negative definite, implying that the system approaches the invariant set. ■

IV. State Estimation

The bearing-to-obstacle will be measured in the vehicle frame. However, the obstacle location is in the camera frame must be rotated to the vehicle frame. If we assume pitch is close to zero, then only the roll angle of the MAV needs to be considered. The rotation to remove the roll angle and rotate the obstacle location to the vehicle frame is

$$\begin{pmatrix} L_{newx} \\ L_{newy} \end{pmatrix} = \begin{pmatrix} \cos\phi & -\sin\phi \\ \sin\phi & \cos\phi \end{pmatrix}\begin{pmatrix} L_x \\ L_y \end{pmatrix}, \quad (14)$$

where $\mathbf{L}$ is location of the obstacle in the image plane. The bearing-to-obstacle η is

$$\eta = \tan^{-1}\left(\frac{L_{newx}}{f}\right), \quad (15)$$

where f is the focal length of the camera.

A range-to-obstacle estimate is extracted from the equations of motion. Solve equation (5) for ρ,

$$\rho_r = \frac{V_a\sin\eta_r}{\dot{\psi} + \dot{\eta}_r}, \quad (16)$$

$$\rho_l = \frac{V_a\sin\eta_l}{\dot{\psi} + \dot{\eta}_l}. \quad (17)$$

Equations (16) and (17) have three problems. 1) The range-to-obstacle estimate was derived using the dynamics equations, hence the dynamics equations cannot be used to estimate $\dot{\eta}_m$ and $\dot{\psi}$ for these equations. Estimates for $\dot{\eta}_*$ and $\dot{\psi}$ must be calculated numerically from available sensors. 2) The denominator may be zero, or numerically close to zero, and create an undefined estimate for ρ_*.

The first problem is solved by numerical differentiation and an alpha filter. The second problem is resolved by the following theorem.

Theorem 4.1: If the bearings-to-obstacle of two obstacles are balanced using the guidance strategy in equation (12), then the denominators $\dot{\psi} + \dot{\eta}_r$ and $\dot{\psi} + \dot{\eta}_l$ in the range-to-obstacle estimates will not remain zero.

Proof: Assume the denominator of equation (16) is zero, then $\dot{\eta}_r + \dot{\psi} = 0$ and

$$\dot{\eta}_r = -\dot{\psi}. \quad (18)$$

Substituting equation (5) into (18) yields

$$\frac{V}{\rho_r}\sin\eta_r - \dot{\psi} = -\dot{\psi}$$
$$\frac{V}{\rho_r}\sin\eta_r = 0$$
$$\eta_r = 0.$$

The only set for which the denominator is zero is when $\eta_r = 0$, or the right obstacle is on the vertical axis of the camera field of view. While this is possible, the obstacle will not be maintained at $\eta_r = 0$ because the Lyapunov function in equation (13) proves that

$$\begin{aligned} \eta_m &\to 0, \\ \frac{\eta_r + \eta_l}{2} &\to 0, \\ \eta_r &\to \eta_l. \end{aligned} \tag{19}$$

If $\eta_r = 0$, then $\eta_l \neq 0$, hence the control will move η_r away from zero. If $\eta_r \neq 0$, then $\dot{\eta}_r \neq -\dot{\psi}$ and the denominator cannot be zero. A similar argument is made for equation (17). ■

V. Simulation

Simulations were conducted in Simulink with a six degree-of-freedom model and full flight dynamics. The camera was simulated parallel to the longitudinal axis of the MAV body frame with a prospective projection. The locations of obstacles in the camera field-of-view were calculated along with the ranges-to-obstacles. The guidance strategy calculates bearings-to-obstacles from their locations in the image plane as discussed in section IV.

The control law in the guidance strategy uses two gains, k_2 to push the obstacles to the edges of the image plane, and k_1 to drive $\rho_d \to 0$. The former is a simple matter of tuning to prevent overshoot while still converging in a reasonable time. The latter balances driving $\eta_m \to 0$ and $\rho_d \to 0$. If the gain is too high, obstacles will go out of the camera field-of-view as the MAV moves to the angle bisector of the two obstacles, and the result will be an oscillation as the obstacles move in and out of the camera field of view. The gain must also allow the control law to maneuver away from the obstacles if $|\rho_d| \gg 0$.

Simulation results for $k_1 = 0.001$, $k_1 = 0.01$, and $k_1 = 0.02$ and shown in figures 3(a), 3(b), and 4(a) respectively. The waypoint path is shown by a dotted line while the trajectory flown is shown by a solid line. In figure 3(a) the trajectory only slightly approaches the perpendicular bisector of the obstacles meaning ρ_d is not driven to zero. Figure 3(b) shows a tendency toward the perpendicular bisector of the obstacles. Figure 4(a) shows a strong tendency toward the perpendicular bisector. The gain from figure 3(b), $k_2 = 0.01$, was chosen for tests.

The purpose of driving $\rho_d \to 0$ is to maneuver the MAV away from obstacles when the approach to the obstacles is at a small angle. This was tested in simulation and shown in figure 4(b). If the guidance strategy were to only drive $\eta_m \to 0$, the MAV would collide with the edges of the obstacle. If $\eta_m \to 0$ and $\rho_d \to 0$, then the MAV will maneuver toward the angle bisector of the obstacles rather than fly between them. The simulation demonstrates the effectiveness of this approach.

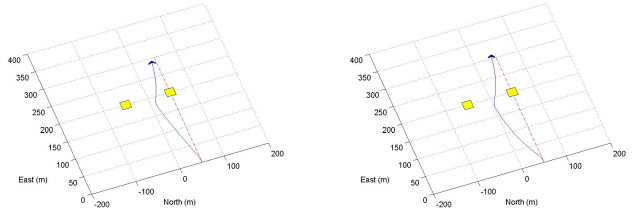

(a) (b)

Fig. 3. a) The guidance strategy is flown in simulation with $k_1 = .001$. The MAV does not approach the perpendicular bisector strongly enough. b) The guidance strategy is flown in simulation with $k_1 = .01$. The MAV approaches the perpendicular bisector slightly.

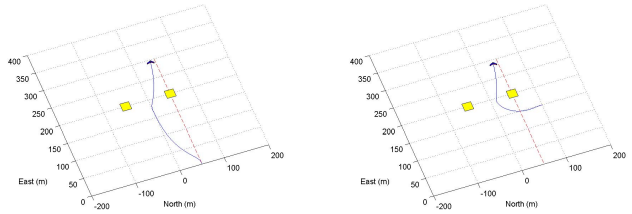

(a) (b)

Fig. 4. a) The guidance strategy is flown in simulation with $k_1 = .02$. The MAV strongly approaches the perpendicular bisector. b) The guidance strategy is flown in simulation with $k_1 = .01$ with an approach to obstacles that must drive $\rho_r - \rho_l \to 0$. The MAV approaches the perpendicular bisector and returns to the waypoint path after passing the obstacles.

VI. Flight Results

Flight tests were conducted using a MAV with a wing span of 48 inches and two eleveon control surfaces as shown in figure 5. The Kestrel autopilot from Procerus Technologies navigated the MAV in flight with control loops for roll, pitch, and yaw. The guidance strategy was processed in MATLAB on the ground station and roll commands transmitted to the autopilot. Obstacles were simulated in Matlab on the ground station.

The trajectory of the MAV in flight test is shown in figure 6. The waypoint path of the MAV is represented by the dashed line and intersects one of the obstacles. The squares are obstacles. To prevent collision, the MAV must maneuver

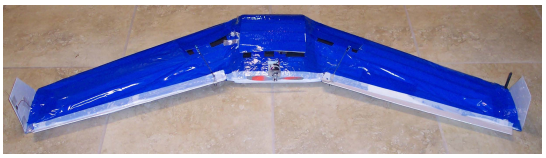

Fig. 5. The MAV flown in flight tests is shown. The wing span is 48 inches with elevons for control surfaces.

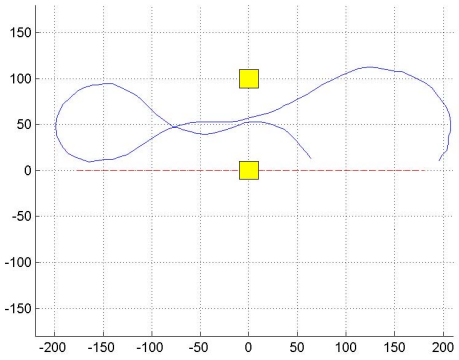

Fig. 6. The flight path of the MAV avoiding two obstacles is shown. The dotted line is the waypoint path and the solid line is the trajectory of the MAV.

away from the waypoint path. The flown trajectory of the MAV is represented by a solid line. The trajectory deviates from the waypoint path and does not intersect either obstacle. The MAV successfully avoids the obstacles in the two passes shown in figure 6.

VII. Conclusion

We have presented a method for reactive obstacle avoidance for multiple obstacles with a guidance strategy based on observations made in the image plane. The obstacles are "pushed" to the edge of the camera field-of-view to avoid collision. Obstacle movement in the image plane provides a means of state estimation. The guidance strategy was successfully demonstrated in simulation and flight.

This paper explores only one tier of the path planning system discussed in the introduction. Future work requires developing and integrating the other tiers of the system into a fully functional obstacle avoidance system. This includes the local path planner and global path planner. Such a system will accomplish all five goals of a trajectory generator.

VIII. Acknowledgements

This research was supported by the Air Force Research Laboratory, Munitions Directorate under SBIR contract No. FA 8651-07-C-0094 to Scientific Systems Company, Inc. and Brigham Young University.

References

[1] N. M. Amato and Y. Wu. A randomized roadmap method for path and manipulation planning. In *Proceedings of the IEEE International Conference on Robotics and Automation*, pages 113–120, Minneapolis, MN, 1996.

[2] Jerome Barraquand, Bruno Langlois, and Jean Claude Latombe. Numerical potential field techniques for robot path planning. *IEEE Transaction On Systems, Man, and Cybernetics*, 22(2):224–241, March/April 1992.

[3] Massimo Bertozzi, Alberto Broggi, and Alessandra Fascioli. Vision-based intelligent vehicles: State of the art and perspectives. *Robotics and Autonomous Systems*, pages 1–16, 2000.

[4] Peng Cheng, Zuojun Shen, and Steven M. LaValle. Using randomization to find and optimize trajectories for nonlinear systems. In *Proceedings of Annual Allerton Conference on Communications, Control, Computing*, 2000.

[5] Emilio Frazzoli, Munther A. Dahleh, and Eric Feron. Real time motion planning for agile autonomous vehicles. *Journal of Guidance, Control, and Dynamics*, 25(1):116–129, January-February 2002.

[6] Ronojoy Ghosh and Claire Tomlin. Maneuver design for multiple aircraft conflict resolution. *Proceedings of the American Control Conference*, June 2000.

[7] Randal Beard Jeffery Saunders. Reactive vidion based obstacle avoidance with camera field of view constraints. *Guidance, Navigation, and Control Conference*, 2008.

[8] L. E. Kavraki, P. Švestka, J.-C. Latombe, and M. Overmars. Probabilistic roadmaps for path planning in high-dimensional configuration spaces. *IEEE Transactions on Robotics and Automation*, 12(4):566–580, 1996.

[9] L.E. Kavraki, M.N. Kolountzakis, and J.-C. Latombe. Analysis of probabilistic roadmaps for path planning. *IEEE Transaction On Robotics and Automation*, 14(1):166–171, Feburary 1998.

[10] Jongcheol Kim and Yasuo Suga. An omnidirectional vision-based moving obstacle detection in mobile robot. *International Journal of Control, Automation, and Systems*, 5(6):663–673, December 2007.

[11] J. J. Kuffner and S. M. LaValle. RRT-connect: An efficient approach to single-query path planning. In *Proceedings of the IEEE International Conference on Robotics and Automation*, pages 995–1001, San Francisco, CA, April 2000.

[12] Jr. Kuffner, J.J. and S.M. LaValle. Rrt-connect: An efficient approach to single-query path planning. *IEEE International Conference on Robotics and Automation*, 2:995–1001, 2000.

[13] S. M. LaValle. Rapidly-exploring random trees: A new tool for path planning. TR 98-11, Computer Science Dept., Iowa State University, October 1998.

[14] S. M. LaValle and J. J. Kuffner. Randomized kinodynamic planning. 20(5):378–400, May 2001.

[15] S. M. LaValle and J. J. Kuffner. Rapidly-exploring random trees: Progress and prospects. In B. R. Donald, K. M. Lynch, and D. Rus, editors, *Algorithmic and Computational Robotics: New Directions*, pages 293–308. A. K. Peters, Wellesley, MA, 2001.

[16] T. Lozano-Perez. Automation planning of manipulator transfer movements. *IEEE Transaction Systems, Man, and Cybernetics*, 11(10):681–698, 1981.

[17] T. Lozano-Perez and M Wesley. An algorithm for planning collision free paths among polyhedral obstacles. *Communication of the ACM*, 22(10):560–570, 1979.

[18] Javier Minguez and Luis Montano. Nearness diagram (nd) navigation: Collision avoidance in troublesome scenarios. *Transactions on Robotics and Automation*, 20(1):45–59, February 2004.

[19] P. O'Dunlaing and C Yap. A retraction method for planning the motion of a disc. *Journal of Algorithms*, 6(1):104–111, 1982.

[20] I. Ohya, A. Kosaka, and A. Kak. Vision-based navigation by a mobile robot with obstacle avoidanceusing single-camera vision and ultrasonic sensing. *IEEE Transactions on Robotics and Automation*, 14(6):969–978, August 1998.

[21] A. Richards and J.P. How. Aircraft trajectory planning with collision avoidance using mixed integer linear programming. *American Control Conference, 2002. Proceedings of the 2002*, 3:1936– 1941, 2002.

[22] Mitul Saha and Jean-Claude Latombe. Finding narrow passages with probabilistic roadmaps: the small step retraction method. pages 622–627. International Conference on Intelligent Robots and Systems, August 2005.

[23] Zheng Sun, David Hsu, Tingting Jiang, Hanna Kurniawati, and John H. Reif. Narrow passage sampling for probabilistic roadmap planning. *IEEE Transactions on Robotics*, 21(6):1105–1115, December 2005.

[24] H.G. Tanner, S.G. Loizou, and K.J. Kyriakopoulos. Nonholonomic navigation and control of cooperating mobile manipulators. *IEEE Transactions on Robotics and Automation*, 19(1):53–64, February 2003.

[25] P. Vadakkepat, Kay Chen Tan, and Wang Ming-Liang. Evolutionary artificial potential fields and their application in real time robot path planning. *Proceedings of the 2000 Congress on Evolutionary Computation*, 1:256–263, July 2000.

[26] David Zhu and Jean Claude Latombe. New heuristic algorithms for efficient hierarchical path planning. *IEEE Transaction On Robotics and Automation*, 7(1):9–20, August 1991.